A Synoptic View of the Third Uniform California Earthquake Rupture Forecast (UCERF3)

Edward H. Field, Thomas H. Jordan, Morgan T. Page, Kevin R. Milner, Bruce E. Shaw, Timothy E. Dawson, Glenn P. Biasi, Tom Parsons, Jeanne L. Hardebeck, Andrew J. Michael, Ray J. Weldon II, Peter M. Powers, Kaj M. Johnson, Yuehua Zeng, Peter Bird, Karen R. Felzer, Nicholas van der Elst, Christopher Madden, Ramon Arrowsmith, Maximilian J. Werner, Wayne R. Thatcher, and David D. Jackson

Resubmitted to SRL

Abstract

Probabilistic forecasting of earthquake-producing fault ruptures informs all major decisions aimed at reducing seismic risk and improving earthquake resilience. Earthquake forecasting models rely on two scales of hazard evolution: long-term (decades to centuries) probabilities of fault rupture, constrained by stress renewal statistics, and short-term (hours to years) probabilities of distributed seismicity, constrained by earthquake clustering statistics. Comprehensive datasets on both hazard scales have been integrated into the Uniform California Earthquake Rupture Forecast, Version 3. UCERF3 is the first model to provide self-consistent rupture probabilities over forecasting intervals from less than an hour to more than a century, and the first capable of evaluating the short-term hazards due to multi-event sequences of complex faulting. This paper gives an overview of UCERF3, illustrates the short-term probabilities with aftershock scenarios, and draws some valuable scientific conclusions from the modeling results. In particular, seismic, geologic, and geodetic data, when combined in the UCERF3 framework, reject two types of fault-based models: long-term forecasts constrained to have local Gutenberg-Richter scaling and short-term forecasts that lack stress relaxation by elastic rebound.

Introduction

More than a century of searching has failed to identify diagnostic precursory signals that can reliably predict the occurrence of large earthquakes (Jordan et al., 2011). However, observed seismic activity can constrain the probabilities of future earthquakes at two scales of hazard evolution, the short-term decay of aftershocks caused by abrupt stress perturbations during rupture (e.g., Reasenberg and Jones, 1989), and the long-term delay needed to reload fault stress after elastic rebound (e.g., WGCEP, 1988). Consistent modeling across both scales of stress evolution is a key requirement for operational earthquake forecasting in seismically active regions (Jordan et al., 2011). The societal need for such models has been underscored by the extensive damage and loss of life resulting from multi-event sequences in Japan, New Zealand, and Italy during the last year alone.

The tectonic reloading of stress by steady block motion, originally postulated by H. F. Reid in his elastic rebound theory (Reid, 1911) and later explained by plate tectonics, has been the basis for a series of fault-specific rupture forecasts developed by the Working Group on California Earthquake Probabilities (e.g., WGCEP, 1988, 2003). California's San Andreas fault system releases most of the plate-boundary strain in strike-slip earthquakes with moment magnitudes M greater than 7.5 and recurrence intervals of a century or more. WGCEP has represented successive large ruptures of a fault by a renewal process with a distribution of inter-event times calibrated against historic and paleoseismic data, using the date of the last event, where it is known, to condition the probability of the next event.

The preceding WGCEP model, UCERF2, restricted fault slip events to full ruptures of predefined fault segments and some contiguous combinations (Field et al., 2009). Moreover, it

generally excluded the possibility of ruptures jumping from one fault to another nearby fault, a phenomenon observed in California and other highly interconnected fault systems (e.g., Wesnousky, 2006). UCERF2 also over-predicted the rate of $6.5 \leq M \leq 7.0$ earthquakes relative to historical seismicity. This "intermediate-magnitude bulge" was reduced relative to previous California models (Frankel et al., 2002), but a discrepancy remained, which WGCEP hypothesized to be an artifact of the segmentation assumptions restricting multi-fault ruptures (Field et al., 2009).

A different class of models, based on aftershock statistics, has been developed for assessing short-term changes in seismic hazard. Examples include the Reasenberg-Jones model (Reasenberg and Jones, 1988, 1994), the Short-Term Earthquake Probability (STEP) model (Gerstenberger et al., 2005), and Epidemic-Type Aftershock Sequence (ETAS) models (Ogata, 1988; Helmstetter and Sorenette, 2002). Earthquake activity is represented as a stochastic point process that obeys the observed power-law scaling of aftershock excitation with mainshock size and aftershock decay in space and time (Omori-Utsu statistics). Each event is marked by a moment magnitude *M* independently drawn from a fixed magnitude-frequency distribution (MFD), usually in the Gutenberg-Richter (GR) form: $\log N = a - bM$, where N is the expected number of events and $b \approx 1$. STEP uses the Reasenberg-Jones model to forecast average aftershock rate from pre-identified mainshocks, whereas ETAS models aftershocks via Monte Carlo simulations, in which every earthquake is a mainshock with its own aftershocks, explicitly accounting for multiple generations of triggered seismicity ("epidemics"). In both types of models, aftershocks can be larger than the mainshock.

These aftershock models ignore proximity to known faults when specifying the probability of triggering large earthquakes. In addition, aftershock decay and stress-renewal delay exhibit

opposing statistical behaviors with conflicting hazard implications. According to Omori-Utsu clustering, the most likely place for the next event is the location of the most recent one; according to Reid renewal, the least likely fault to rupture is the one that ruptured most recently. Omori-Utsu sequences of aftershocks are more clustered than a Poisson process, whereas Reid sequences of elastic rebounds are more periodic. The new forecasting framework represented in UCERF3 merges these opposing behaviors into a consistent multiscale model by conditioning the short-term ETAS forecast on the long-term Reid forecast.

Uniform California Earthquake Rupture Forecast, Version 3 (UCERF3)

The model comprises three levels of forecasting: a time-independent model, UCERF3-TI (Field et al., 2014); a long-term, time-dependent refinement based on Reid-renewal statistics, UCERF3-TD (Field et al., 2015); and a short-term clustering model, based on ETAS statistics, UCERF3-ETAS (Field et al., 2017). The model is hierarchical in the sense that the TD probabilities are conditioned on the TI model, and the ETAS probabilities are conditioned on the TD model (Figure 1).

UCERF3-TI gives the long-term rates of all earthquakes with $M \geq 2.5$ throughout the California region. Target earthquakes are of two types: "supraseismogenic" ruptures on modeled faults with $M \geq M_{ss}$, where M_{ss} the minimum magnitude of a rupture spanning the seismogenic layer, and "gridded seismicity" from MFDs assigned on a $0.1^{o} \times 0.1^{o}$ geographic mesh. All faults were divided into small subsections with along-strike lengths of about half the down dip width, typically ~7km (Figure 1a). Fault-based ruptures were defined by sets of two or more contiguous subsections, corresponding to $M_{ss} \approx 6.3$. We omitted ruptures that jumped fault gaps exceeding 5 km, a value consistent with the limited observations (Wesnousky, 2006) and supported by rupture simulations (e.g., Harris et al., 1991), and we excluded those that failed a

stress-compatibility test. The number of fault-based ruptures in UCERF3 is ~250,000 compared to ~8,000 in UCERF2. The magnitude of each rupture was computed from empirical scaling relations that relate moment magnitude to rupture area.

A system-wide "grand inversion" simultaneously determined the rates of all ruptures by minimizing a quadratic objective function measuring the model's misfit to fault slip rates, paleoseismic event rates, and observed seismicity. This underdetermined problem was regularized by smoothness conditions and solved by simulated annealing under appropriate positivity constraints (Page et al., 2014). The inversion approach was less prescriptive than previous methodologies; e.g., it determined the range of MFDs most consistent with available data, rather than assuming a functional form. As expected, relaxing fault segmentation and allowing multi-fault ruptures eliminated the intermediate-magnitude over-prediction (bulge) evident in UCERF2; the consequent transfer of moment release to larger magnitudes increased the 30-year, statewide probability of a $M \geq 8$ earthquake from 4.7% to 7.0%. Other improvements included a revised, more extensive model of active California faults and the inclusion of kinematically consistent deformation models that assimilated both geodetic and geologic data in estimating fault slip rates (Parsons et al., 2013). UCERF3-TI implies that about two thirds of deformation not attributed to defined faults goes into permanent strain not described by purely elastic behavior.

The model was evaluated by applying quantitative and visual measures of its fit to independent data subsets, which were then assessed by expert panels. Expert opinion was also elicited in weighting the 1440 branches of the logic tree used to represent the UCERF3-TI epistemic uncertainties. The hazard obtained by combining the UCERF3-TI model with ground-

117 motion prediction equations has been incorporated into the 2014 revisions of the National
118 Seismic Hazard Maps (Petersen et al., 2014).
119 UCERF3-TD was built by augmenting UCERF3-TI with a composite Reid renewal model
120 that conditioned the rupture probabilities on the "open interval", defined as the time since a fault
121 subsection last participated in a supraseismogenic event. In UCERF2, the renewal model could
122 be enforced at the fault-segment level, and the probabilities were balanced to approximate slip
123 rates on a fault-by-fault basis (Field et al., 2009). To relax segmentation and include multi-fault
124 ruptures, it was necessary to enforce the UCERF3 renewal statistics at the fault-subsection level
125 and to balance the probabilities at the fault-system level. This was accomplished by a system-
126 wide averaging algorithm that accounted for the variability of the recurrence and open intervals
127 among the fault subsections involved in a specified rupture. On many faults, the date of the last
128 supraseismogenic event is unknown. It is unlikely, however, that such events could have
129 occurred in California without detection after 1875; hence, a 140-year "historic open interval"
130 was used as a lower bound on the date-of-last-event, allowing time-dependent probabilities to be
131 cast for all fault-based ruptures. The renewal model also incorporated magnitude-dependent
132 aperiodicity factors that adjusted the inter-event times of smaller events to be more variable than
133 that of larger ones. Epistemic uncertainties were represented by four levels of temporal
134 predictability specified by aperiodicity factors of a Brownian passage time model (WGCEP,
135 2003) ranging from 0.4 to 1.0.
136 Compared to the TI model, TD probabilities are relatively low on faults where a large event
137 has recently occurred and relatively high where the time since last event exceeds the average
138 recurrence interval (Figure 1b). Places where the rupture probabilities are high compared to the
139 time-independent model include the San Andreas Fault in southern California and the Hayward-

Rogers Creek Fault in northern California, which both show probability gains of about a factor of two.

UCERF3-ETAS represents spatiotemporal clustering, including aftershocks and other triggered earthquake activity, discretized onto a ~2-km mesh. The forecasting statistics for an interval $0 < t \leq T$ are computed from large sets of $M \geq 2.5$ catalogs simulated within the TD framework. Each simulation is initialized at $t = 0$ with an observed or hypothetical $M \geq 2.5$ catalog of past earthquakes. Every earthquake, observed or simulated, is allowed to trigger a set of first-generation aftershocks by Monte Carlo sampling from an ETAS model that has spatial and temporal kernels calibrated to California seismicity (Hardebeck, 2013); they in turn trigger second-generation aftershocks, and so-on for all subsequent generations up to time *T*. Earthquakes that occur spontaneously according to UCERF3-TD probabilities, typically ~30% of the total, also trigger aftershocks.

In UCERF3-ETAS, the probabilities of all fault-based supraseismogenic ruptures, including aftershocks, are conditioned by Reid renewal statistics that evolve during the seismic sequence; i.e., the probability of a fault subsection participating in a future event is reduced if that subsection has already participated in a previous event of the sequence. The explicit inclusion of elastic rebound in modeling earthquake sequences is essential to the stability of the UCERF3-ETAS model, as discussed below.

The probabilities of large aftershocks ($M \geq 6.7$) in the week following a scenario $M7$ rupture of the Mojave section of the San Andreas Fault are mapped in Figure 1c as probability gains relative to UCERF3-TD. Relatively high gains (up to ~100) extend spatially along nearby faults, not just the high-rate San Andreas but also low-rate faults such as the Cucamonga and Garlock.

A wide variety of metrics for forecasting hazard and loss can be derived from UCERF3-ETAS model, including the likelihood of large earthquakes during multi-event sequences of complex faulting. The number of Monte Carlo simulations needed to obtain stable forecast estimates depends on the metric of interest. Estimates in this paper were derived from ensembles of 10^4 to 4×10^5 catalogs.

Figure 2 shows the UCERF3-ETAS aftershock forecast following a $M6.1$ earthquake on the Parkfield section of the San Andreas Fault and compares it with an equivalent one from an ETAS model that lacks faults. Aftershock nucleation in the former extends along the major faults of the San Andreas system, unlike the smooth, isotropic distribution forecast by the ETAS point-process model. This scenario is particularly interesting because a M6.1 foreshock is known to have occurred near Parkfield about two hours before the 1857 Fort Tejon earthquake, an $M7.8$ rupture that propagated down the San Andreas from Parkfield to Cajon Pass (Sieh, 1978; Meltzner and Wald, 1999). According to UCERF3-ETAS, in the first week following the $M6.1$ initial event, the average probability of a $M \geq 7.8$ rupture extending southeastward along the San Andreas to the Mojave South section is 5.8×10^{-3}. In contrast, the probability of a $M \geq 7.8$ rupture extending northwestward through the creeping section to the Peninsula section is 4.0×10^{-4}, more than an order of magnitude lower. The isotropic probability of a $M \geq 7.8$ aftershock from the no-fault ETAS model is 1.2×10^{-3}.

The hierarchical UCERF3 model is complex, and its substantial epistemic uncertainties have yet to be fully investigated. We can nevertheless identify two types of forecasting models within the UCERF3 framework that are rejected by the UCERF3 datasets: long-term models with local GR scaling and short-term models without stress relaxation (elastic rebound).

Inadequacy of Local Gutenberg-Richter Scaling

Below some outer scale $M_{\max}$, the total seismicity of a region as large as northern or southern California can be well described by a Gutenberg-Richter magnitude-frequency distribution (GR-MFD) with a *b*-value near unity (Felzer, 2013). There has been considerable debate, however, about whether a GR-MFD applies in small regions of high-rate faulting (Ishibe and Shimazaki, 2012; Kagan et al., 2012). An alternative is the "characteristic MFD" hypothesis, stating that the rate of supraseismogenic ruptures on major faults such as the San Andreas is elevated above the GR extrapolation of the small-magnitude seismicity (Youngs and Coppersmith, 1985).

We tested these competing hypotheses by inverting the earthquake-rate data with and without local GR-MFD constraints. Unconstrained inversions obtain acceptable models in which the MFDs of some faults are characteristic while others are "anti-characteristic"; i.e., depleted in large earthquakes relative to the GR extrapolation (e.g. Figure 3a). This behavior can be measured by a characteristic factor, C_M, defined as the cumulative rate of ruptures above some supraseismogenic magnitude $M \geq M_{ss}$, here taken to be 7.0, divided by the extrapolated GR rate. The empirical distribution of C_7 across all subsections has a mean value of 2.18 and a standard deviation of 2.21. More subsections are strongly characteristic (37% with $C_7 > 2.0$) than strongly anti-characteristic (20% with $C_7 < 0.5$). The C_7 values show a positive correlation with moment release; weighting subsections by their moment rates increases the C_7 mean to 3.20. No model with a narrow distribution of C_7 about unity, as required by the local GR hypothesis, produced acceptable fits to the observed fault slip rates and regional event rates (Field et al., 2014).

The UCERF3-TI dataset thus strongly favors the characteristic-MFD hypothesis over the local GR hypothesis. The model corrects for the aseismic creep rate measured locally across

207 faults (Weldon et al., 2013), as well as the aseismic deformation derived from the geodetic and
208 geologic modeling (Parsons et al., 2013). The corrected slip rates require, on average,
209 significantly higher rates of large earthquakes than predicted by local GR scaling. Explaining the
210 discrepancy in terms of aseismic slip would require a 50% reduction in the average seismic slip
211 rate or a 50% over-prediction of the regional seismicity rates. The former was rejected as a
212 viable alternative by the UCERF3 expert review panel (Field et al., 2014); the latter was rejected
213 by a one-sided test against the empirical MFD for California at the 97.5% confidence level
214 (Felzer, 2013).

215 In Figure 3, we compare aftershocks in the week following a $M4.8$ mainshock near the
216 southern end of the Coachella section of the San Andreas Fault (characteristic MFD, $C_7 = 5.8$)
217 with those from a M 4.8 mainshock on the Borrego segment of the San Jacinto Fault (anti-
218 characteristic MFD, $C_7 = 0.25$). The corresponding probabilities that these events will trigger
219 one or more $M \geq 7.0$ aftershocks are 1.7×10^{-3} and 7.4×10^{-5}, respectively, compared to a GR
220 probability of 3.3×10^{-4}. The probability gains relative to GR, 5.1 and 0.22, directly reflect the
221 characteristic factors. In general, the magnitude distribution of short-term aftershocks from a
222 small mainshock near an active fault is governed by that fault's long-term magnitude probability
223 distribution (Michael, 2012).

224 For both examples in Figure 3, the UCERF3-TD characteristic factors deviate from unity by
225 more than the UCERF3-TI characteristic factors ($C_7 = 2.1$ and 0.41), illustrating the direct effect
226 of the long-term renewal model on the short-term probabilities. For the Coachella section, where
227 the last large earthquake occurred over 300 years ago, the gain is significant even at small
228 magnitudes; i.e., the one-week probability of one or more $M \geq 4.8$ aftershocks is 0.091,

compared to the standard GR value of 0.05 often used as a seismological rule-of-thumb (Reasenberg and Jones, 1994).

The Need for Elastic Rebound

The applicability of elastic rebound in earthquake forecasting remains controversial (Kagan et al., 2012; Tormann et al, 2015; Bürgmann et al., 2016; Mulargia et al., 2016). In UCERF3-TD, elastic rebound is modeled as a Reid renewal process in which rupture of a fault subsection instantaneously reduces the probability of that subsection participating in a future rupture. If we do not include this elastic rebound in UCERF3-ETAS, the model does not produce realistic earthquake sequences. The ETAS probability density of triggering a new rupture increases with proximity to an old rupture; hence, without a renewal mechanism for lowering the rupture probability, the most likely subsection to rupture is one that has just ruptured. Sequences are then dominated by recurring re-ruptures of the same fault area, which is not observed in nature (Field et al., 2017). Motivated by earlier assertions of this issue (Field, 2011), van der Elst and Shaw (2015) subsequently found that aftershocks larger than the main shock tend to nucleate in the outer regions of the parent aftershock zone, which they interpreted as the inhibition of re-rupturing by stress relaxation.

In UCERF3 simulations, elastic rebound is required to inhibit re-ruptures of faults with characteristic factors as low as unity (i.e., with GR MFDs). Moreover, aftershock sequences near faults with even moderately characteristic MFDs can become unstable without it. Hardebeck's (2013) calibration of ETAS parameters using regional California earthquake catalogs yields an effective branching ratio near its critical value of unity; on average, each event eventually spawns about one other event over infinite time, which implies that almost all events are triggered and very few are spontaneous. When these regional statistics are applied in the vicinity

252 of faults with high characteristic factors, the local branching ratio exceeds unity, and the
253 sequences exhibit explosive exponential growth. The application of elastic rebound tames this
254 unrealistic growth by lowering the characteristic factor after a rupture.
255 Figure 4 illustrates the average one-week aftershock nucleation frequencies in the Los
256 Angeles region following a $M7.0$ scenario on the Mojave section of the San Andreas Fault and in
257 the San Francisco region for a $M7.1$ scenario on the Hayward Fault. The former is the same as in
258 Figure 1c, and the latter is similar to the scenario used by the U.S. Geological Survey in its
259 "Haywired" preparedness study
260 (https://www2.usgs.gov/natural_hazards/safrr/projects/haywired.asp, last accessed on April 27,
261 2017). The aftershock distributions are again extended along the major faults. The aftershock
262 MFDs show probability gains of up to more than two orders of magnitude relative to UCERF3-
263 TD, and their shape differences reflect the characteristic factors and open intervals of the nearby
264 faults.
265 Figure 4 also illustrates the influence of one important uncertainty—the extent to which
266 smaller aftershocks occurring on the mainshock rupture surface can trigger large fault ruptures.
267 The darker colored bands in Figures 3 and 4 show the range bracketed by the two end-member
268 hypotheses (triggering allowed, or not). The difference can be up to an order of magnitude for
269 the $M7$ Mojave scenario. Limited observations suggest that such triggering is suppressed on
270 recently ruptured faults (van der Elst and Shaw, 2015), but the evidence is far from conclusive
271 with respect to larger ruptures. We have therefore equally weighted these two possibilities to
272 obtain the mean values (solid lines) in Figures 3 and 4.

Discussion

The hierarchical and modular structure of UCERF3 provides a self-consistent framework for earthquake forecasting across the complete range of temporal and spatial scales, from aftershocks during the first hours following small, spatially distributed events to the largest earthquakes expected on the San Andreas fault system over intervals of many decades. Relaxation of fault segmentation and allowance of multi-fault ruptures substantially increases the complexity and multiplicity of possible ruptures, reducing the characteristic factors near faults and improving agreement with observed seismicity.

Previous fault-based models have not included aftershocks and other manifestations of earthquake clustering, and ETAS point-process models have not accounted for known faults or stress relaxation during rupture. The novel coupling of Omori-Utsu clustering statistics to Reid renewal statistics permits the estimation of earthquake triggering probabilities conditioned by the proximity of events to active faults, and the resulting model is capable of representing the short-term hazards due to multi-event sequences of complex faulting. The model can be updated with observed seismicity to capture the static or dynamic triggering effects that play out during a particular sequence. The multiscale framework is adaptable to many other continental fault systems, and the short-term component should be applicable to the forecasting of induced seismicity.

UCERF3 is under evaluation by the U. S. Geological Survey as a prototype component of an operational earthquake forecasting system (Field et al., 2016). Proposed validation steps include prospective testing of UCERF3 in the Collaboratory for the Study of Earthquake Predictability (Zechar et al., 2010), evaluation of its consistency with earthquake sequences observed in similar tectonic environments, and comparison of its forecasts with those derived from physics-based

earthquake simulators. Figure 5 shows an example application to the southeastern end of the San Andreas Fault, where the occurrence of small earthquakes in 2009 and 2016 prompted alerts by the California Office of Emergency Services (Jordan and Jones, 2010). The UCERF3-ETAS probability gains decay rapidly, dropping from two orders of magnitude in the first hour to one order of magnitude over the first week for the 2009 event, which raises the question of model valuation. Earthquake forecasts possess no intrinsic societal value; rather, they acquire value through their ability to influence decisions made by the public and decision-makers seeking to mitigate seismic risk (Jordan et al., 2011). The value of the UCERF3 short-term forecasts will need to be scertained in the context of specific applications.

Data and Resources

All simulation data presented in this paper are available from http://www.WGCEP.org/UCERF3-ETAS (last accessed March 2017) and all calculations were made using OpenSHA (http://www.OpenSHA.org; last accessed March 2017), which in turn utilizes Generic Mapping Tools (http://gmt.soest.hawaii.edu ; last accessed January 2012) and JFree-Chart (http://www.jfree.org/jfreechart/ ; last accessed March 2012) for making plots.

Acknowledgments

UCERF3 development was supported by the California Earthquake Authority, U. S. Geological Survey, USGS-SCEC Cooperative Agreement G12AC20038, and NSF-SCEC Cooperative Agreement EAR-1033462. Calculations were performed at the Texas Advanced Computing Center and the USC Center for High-Performance Computing and Communications. We thank the USGS Powell Center for Analysis and Synthesis for supporting workshops on UCERF3-ETAS development. We also thank Michael Blanpied, Matt Gerstenberger, and an

anonymous individual for constructive review comments. The Southern California Earthquake Center contribution number for this paper is 7165.

References

Bürgmann, R., Uchide, N., Hu, Y., Matsuzawa, T. (2016). Tohoku rupture reloaded?, *Nat. Geosci.* **9**, 183-184.

Felzer, K. R. (2013). Appendix K: The UCERF3 earthquake catalog, *U.S. Geol. Surv. Open-File Rept. 2013-1165*-K, and *California Geol. Surv. Special Rept. 228*-K.

Field, E. H., T. E. Dawson, K. R. Felzer, A. D. Frankel, V. Gupta, T. H. Jordan, T. Parsons, M. D. Petersen, R. S. Stein, R. J. Weldon II and C. J. Wills (2009). Uniform California Earthquake Rupture Forecast, Version 2 (UCERF 2), *Bull. Seismol. Soc. Am.*, **99**, 2053-2107, doi:10.1785/0120080049.

Field, E.H. (2011). Aftershock Statistics Constitute the Strongest Evidence for Elastic Rebound in Large Earthquakes, *Abstract S22B-08 presented at 2011 Fall Meeting, AGU*, San Francisco, CA, 5-9 Dec.

Field, E. H., R. J. Arrowsmith, G. P. Biasi, P. Bird, T. E. Dawson, K. R. Felzer, D. D. Jackson, K. M. Johnson, T. H. Jordan, C. Madden, A. J. Michael, K. R. Milner, M. T. Page, T. Parsons, P. M. Powers, B. E. Shaw, W. R. Thatcher, R. J. Weldon, and Y. Zeng (2014). Uniform California Earthquake Rupture Forecast, version 3 (UCERF3)—The time-independent model, *Bull. Seism. Soc. Am, ,* **104**, 1122-1180, doi: 10.1785/0120130164.

Field, E. H., R. J. Arrowsmith, G. P. Biasi, P. Bird, T. E. Dawson, K. R. Felzer, D. D. Jackson, K. M. Johnson, T. H. Jordan, C. Madden, A. J. Michael, K. R. Milner, M. T. Page, T. Parsons, P. M. Powers, B. E. Shaw, W. R. Thatcher, R. J. Weldon, and Y. Zeng (2015). Long-Term, Time-Dependent Probabilities for the Third Uniform California Earthquake Rupture Forecast (UCERF3), *Bull. Seism. Soc. Am.* **105**, 511–543, doi: 10.1785/0120140093.

Field, E. H. T. H. Jordan, L. M. Jones, A. J. Michael, M.l L. Blanpied, and Other Workshop Participants (2016). The Potential uses of Operational Earthquake Forecasting, *Seismol. Res. Lett.* **80**, 1-10. doi: 10.1785/0220150174.

Field, E. H., K. R. Milner, J. L. Hardebeck, M. T. Page, N. van der Elst, T. H. Jordan, A. J. Michael, B. E. Shaw, and M. J. Werner (2017). A Spatiotemporal Clustering Model for the Third Uniform California Earthquake Rupture Forecast (UCERF3-ETAS): Toward an Operational Earthquake Forecast, *Bull. Seism. Soc. Am.* **107**, ???-???, doi: 10.1785/0120160173.

Frankel, A. D., M. D. Petersen, C. S. Mueller, K. M. Haller, R. L. Wheeler, E. V. Leyendecker, R. L. Wesson, S. C. Harmsen, C. H. Cramer, D. M. Perkins, K. S. Rukstales (2002). Documentation for the 2002 update of the national seismic hazard map, *U.S. Geol. Surv. Open-file Report 2002-420*.

Gerstenberger, M., S. Wiemer, L. M. Jones, and P. A. Reasenberg (2005), Real-time forecasts of tomorrow's earthquakes in California, *Nature*, ***435***, 328-331.

Hardebeck, J. L. (2013). Appendix S: Constraining Epidemic Type Aftershock Sequence (ETAS) Parameters from the Uniform California Earthquake Rupture Forecast, Version 3 Catalog and

Validating the ETAS Model for Magnitude 6.5 or Greater Earthquakes, *U.S. Geol. Surv. Open-File Rept. 2013-1165*-S, and *California Geol. Surv. Special Rept. 228*-S.

Harris, R.A., R.J. Archuleta, and S.M. Day (1991). Fault steps and the dynamic rupture process: 2-D numerical simulations of a spontaneously propagating shear fracture, *Geophys. Res. Lett.*, **18**, 893-896.

Helmstetter, A., D. Sornette (2002). Sub-critical and supercritical regimes in epidemic models of earthquake aftershocks, *J. Geophys. Res.*, **107**, 2237.

Ishibe, T., K. Shimazaki (2-12). Characteristic earthquake model and seismicity around late Quaternary active faults in Japan, *Bull. Seismol. Soc. Am.,* **102**, 1041-1058.

Jordan, T. H., and L. M. Jones (2010). Operational earthquake forecasting: some thoughts on why and how, *Seism. Res. Lett.* **81** (4), 571–574.

Jordan, T. H., Y.-T. Chen, P. Gasparini, R. Madariaga, I. Main, W. Marzocchi, G. Papadopoulos, G. Sobolev, K. Yamaoka, and J. Zschau (2011). Operational earthquake forecasting: state of knowledge and guidelines for implementation, final report of the International Commission on Earthquake Forecasting for Civil Protection, *Annals Geophys.*, **54**(4), 315-391, doi:10.4401/ag-5350.

Kagan, Y. Y., D. D. Jackson, and R. J. Geller (2012). Characteristic earthquake model, 1884–2011, RIP, *Seismol. Res. Lett.* **83**, 951–953, doi: 10.1785/0220120107.

Meltzner, A. J. and D. J. Wald (1999), Foreshocks and aftershocks of the great 1857 California earthquake, *Bull. Seismol. Soc. Am.* **89**, 1109–1120

Michael, A. J. (2012a). Fundamental questions of earthquake statistics and estimation of earthquake probabilities from possible forecshocks, *Bull. Seism. Soc. Am.* **102**, 2547-2562, doi: 10.1785/0120090184.

Mulargia, F., P. B. Stark, R. J. Geller, s (2016). Why is Probabilistic Seismic Hazard Analysis (PSHA) Still Used?, Phys. Earth Planet. Int., in pres.

Newcombe, R. G. (1998). Two-sided confidence intervals for the single proportion: comparison of seven methods, *Statistics in Medicine* **17**, 857-872.

Ogata, Y. (1988). Statistical models of point occurrences and residual analysis for point processes, *J. Am. Stat. Assoc.* **83**, 9-27.

Page, M. T., E. H. Field, K. R. Milner, and P. M. Powers (2014). The UCERF3 Grand Inversion: Solving for the Long-Term Rate of Ruptures in a Fault System, *Bull. Seismol. Soc. Am.* **104**, 1181–1204, doi: 10.1785/0120130180.

Parsons, T., K. M. Johnson, P. Bird, J. M. Bormann, T. E. Dawson, E. H. Field, W. C. Hammond, T. A. Herring, R. McCaffrey, Z.-K. Shen, W. R. Thatcher, R. J. Weldon, II, and Y. Zeng (2013). Appendix C: Deformation models for UCERF3.3, *U.S. Geol. Surv. Open-File Rept. 2013-1165*-C, and *California Geol. Surv. Special Rept. 228*-C.

Petersen, M. D. (2014). Documentation for the 2014 Update of the United States National Seismic Hazard Maps, *et al.*, *U. S. Geol. Surv. Open-File Report 2014-1091* (2014), 243 pp.

Reasenberg, P. A., and L. M. Jones (1989). Earthquake hazard after a mainshock in California, *Science* **243**, 1173-1176.

Reasenberg, P., and L. Jones (1994). Earthquake aftershocks: update, *Science* **265**, 1251-1252.

Reid, H. F. (1911). The elastic-rebound theory of earthquakes, *Univ. Calif. Pub. Bull. Dept. Geol. Sci.,* **6**, 413-444.

Sieh, K. E. (1978). Central California foreshocks of the great 1857 earthquake, *Bull. Seismol. Soc. Am.* **68,** 1731–1749.

Tormann, T., Enescu, B., Woessner, J., Wiemer, S., 2015. Randomness of megathrust earthquakes implied by rapid stress recovery after the Japan earthquake. *Nat. Geosci.* **8**, 152–158.

van der Elst, N. J., and B. E. Shaw (2015). Larger aftershocks happen farther away: Nonseparability of magnitude and spatial distributions of aftershocks, *Geophys. Res. Lett.* **42**, 5771-5778, DOI: 10.1002/2015GL064734.

Weldon II, R. J., D. A. Schmidt, L. J. Austin, E. M. Weldon, and T. E. Dawson (2013b). Appendix D: Compilation of creep rate data for California faults and calculation of moment reduction due to creep.

Wesnousky, S. G. (2006). Predicting the endpoints of earthquake fuptures, *Nature* **444**, 358-360, doi:10.1038/nature05275.

Working Group on California Earthquake Probabilities (1988). Probabilities of large earthquakes occurring in California on the San Andreas fault, *U.S. Geological Survey Open-File Report*, p. 62.

Working Group on California Earthquake Probabilities (2003). Earthquake Probabilities in the San Francisco Bay Region: 2002–2031, *USGS Open-File Report 2003-214*.

Youngs, R. R., K. J. Coppersmith (1985). Implications of fault slip rates and earthquake recurrence models to probabilistic seismic hazard estimates, *Bull. Seismol. Soc. Am.* **75**, 939-964.

Zechar, J. D., D. Schorlemmer,M. Liukis, J. Yu, F. Euchner, P. J. Maechling, and T. H. Jordan (2010). The Collaboratory for the Study of Earthquake Predictability perspectives on computational earth science, *Concurrency Computat. Pract. Exper.* **22**, 1836–1847, doi: 10.1002/cpe.1519.

Author Mailing Addresses

Edward H. Field
U.S. Geological Survey, Denver Federal Center
PO Box 25046, MS 966
Denver, CO 80225-0046

Thomas H. Jordan
University of Southern California
Southern California Earthquake Center

3651 Trousdale Parkway #169
Los Angeles, California, 90089-0742

Morgan T. Page
U.S. Geological Survey
525 S. Wilson Avenue
Pasadena, CA 91106

Kevin R. Milner
University of Southern California
Southern California Earthquake Center
3651 Trousdale Parkway #169
Los Angeles, California, 90089-0742

Bruce E. Shaw
Lamont Doherty Earth Observatory
Columbia University
Palisades, NY 10964

Timothy E. Dawson
California Geological Survey
345 Middlefield Road MS 520
Menlo Park, CA 94025

Glenn P. Biasi
University of Nevada Reno
Nevada Seismological Laboratory MS-174
1664 N. Virginia St.
Reno, NV 89557

Tom Parsons
U.S. Geological Survey MS 999
345 Middlefield Road
Menlo Park, CA 94025

Jeanne L. Hardebeck
U.S. Geological Survey MS 977
345 Middlefield Road
Menlo Park, CA 94025

Andrew J. Michael
U.S. Geological Survey MS 977
345 Middlefield Road
Menlo Park, CA 94025

Ray J. Weldon, II

Department of Geological Sciences
University of Oregon
Eugene, OR 97403-1272

Peter M. Powers
U.S. Geological Survey, Denver Federal Center
PO Box 25046, MS 966
Denver, CO 80225-0046

Kaj M. Johnson
Department of Geological Sciences
Indiana University
1001 E. 10th St.
Bloomington, IN 47405

Yuehua Zeng
U.S. Geological Survey, Denver Federal Center
PO Box 25046, MS 966
Denver, CO 80225-0046

Peter Bird
Department of Earth, Planetary, & Space Sciences
University of California
Los Angeles, CA 90095-1567

Karen R. Felzer
U.S. Geological Survey
525 S. Wilson Avenue
Pasadena, CA 91106

Nicholas van der Elst
U.S. Geological Survey
525 S. Wilson Avenue
Pasadena, CA 91106

Christopher Madden
College of Earth, Ocean, and Atmospheric Sciences
Oregon State University
104 CEOAS Administration Building
Corvallis, OR 97331-5503

Ramon J. Arrowsmith
Arizona State University
School of Earth and Space Exploration
PO Box 876004
Tempe, AZ 85287-6004

Maximilian J. Werner
School of Earth Sciences and Cabot Institute
University of Bristol
Wills Memorial Building, Queen's Road
Bristol, BS8 1RJ, United Kingdom

Wayne R. Thatcher
U.S. Geological Survey MS 977
345 Middlefield Road
Menlo Park, CA 94025

David D. Jackson
Department of Earth, Planetary, & Space Sciences
University of California
Los Angeles, CA 90095-1567

Figures

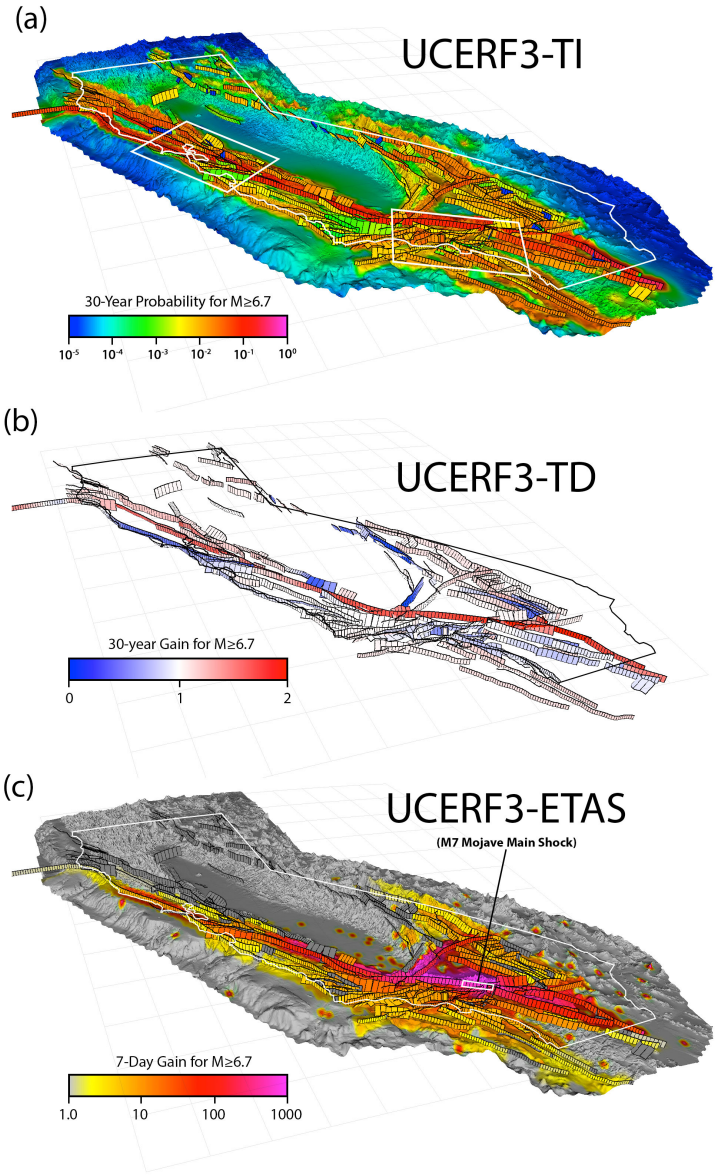

Figure 1. (a) TI probabilities that locations in greater California will participate in one or more $M \geq 6.7$ earthquake ruptures during a 30-year interval. Modeled fault subsections are depicted as black-outlined parallelograms. **(b)** TD participation probability gains relative to TI for $M \geq 6.7$ fault ruptures during the next 30-year interval. **(c)** ETAS probability gains relative to TI for $M \geq 6.7$ earthquakes during a 7-day interval immediately following a $M7$ scenario on the Mojave section of the San Andreas Fault. Main shock rupture area is outlined in white.

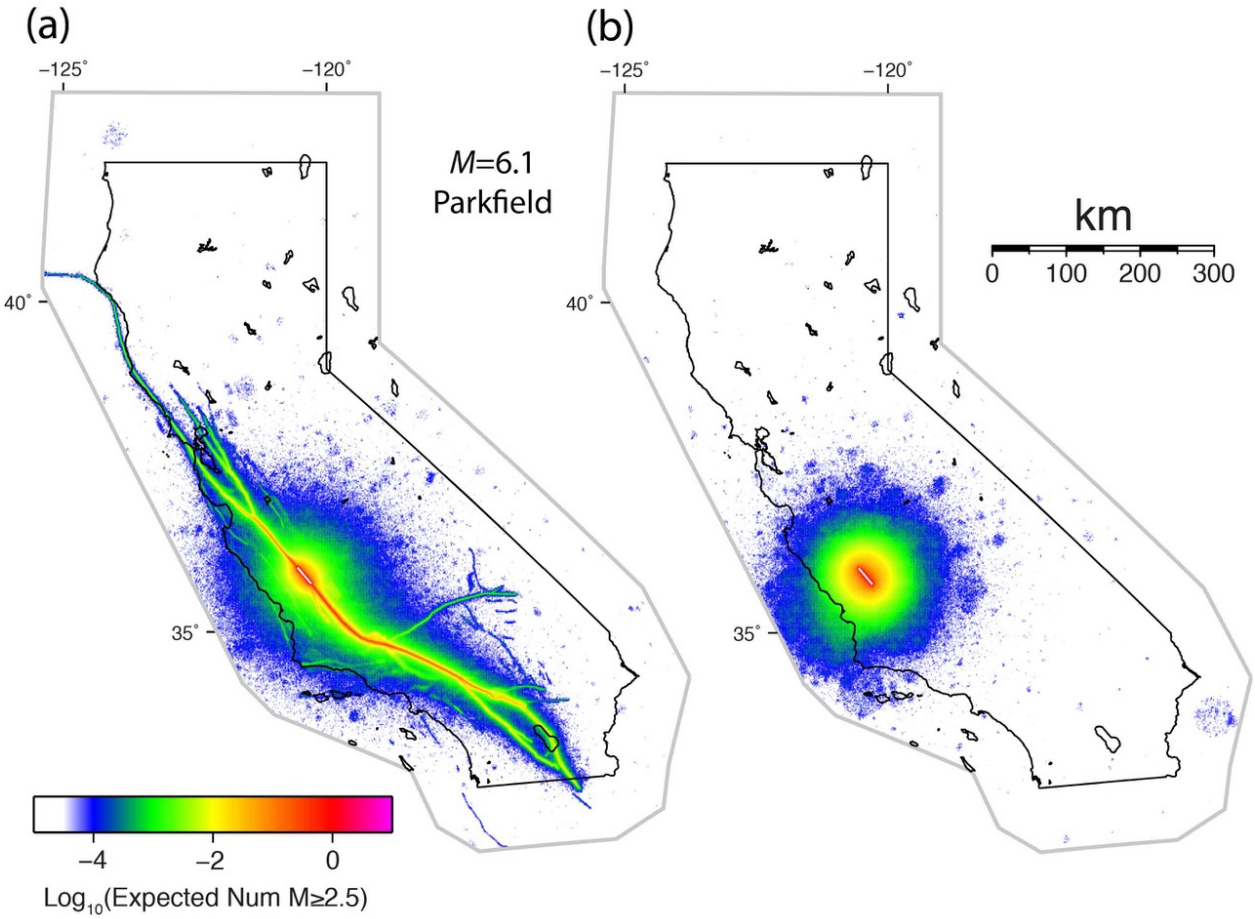

562

563

564 **Figure 2.** (a) Aftershock nucleation rates following a $M6.1$ earthquake on the Parkfield section of the San Andreas
565 Fault, based on 2×10^5 UCERF3-ETAS simulations. Map shows the average number of $M \geq 2.5$ earthquakes
566 nucleating in $0.02^o\times0.02^o$ cells over a 7-day period immediately following the mainshock rupture, which is plotted
567 as a white line. (b) Aftershock nucleation rates following the same $M6.1$ mainshock computed from an equivalent
568 ETAS model with no faults.

569

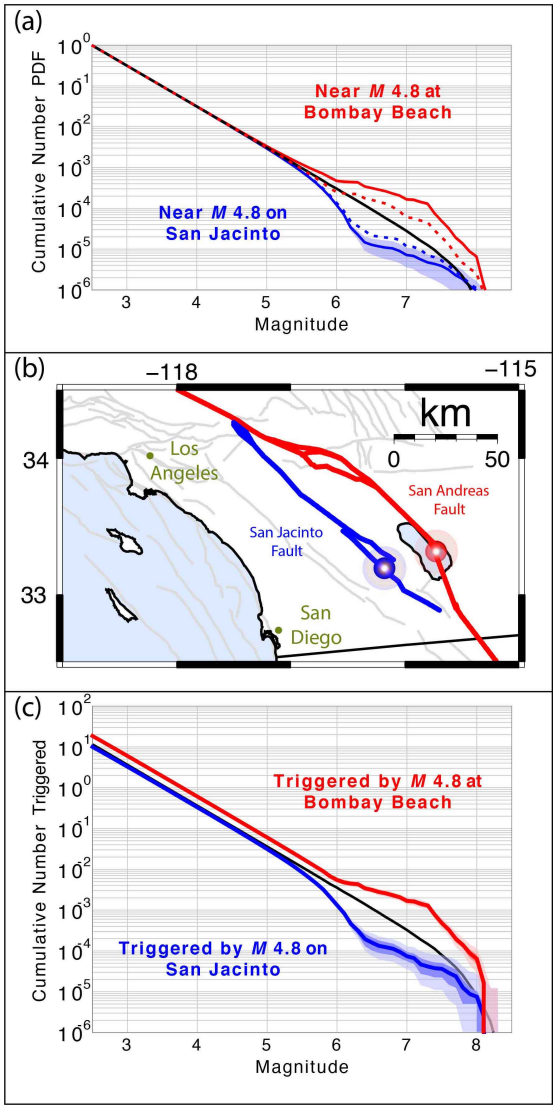

570

571 **Figure 3. (a)** Cumulative, long-term magnitude-frequency distributions for a point near the Coachella section of the
572 San Andreas Fault (red) and the Borrego section of the San Jacinto Fault (blue), compared with the regional GR
573 distribution (black). Distributions for the mean TI model (dotted) and mean TD model (solid colored) are averages
574 of the nearby MFDs weighted by the spatial ETAS kernels centered on the events shown in (B). The shaded bands
575 represent the modeling uncertainties. **(b)** Faults (colored lines) and locations of the $M4.8$ mainshock scenarios (red
576 and blue circles). The Coachella hypocenter is offset about 4 km from the fault terminus to mimic the 03/24/09
577 Bombay Beach event. **(c)** Expected number of aftershocks forecast during the first week following the $M4.8$
578 Coachella and Borrego scenarios (red and blue, respectively), compared to the regional GR model (black line). The
579 dark and light shaded bounds represent modeling and sampling uncertainties, respectively; the latter are from a
580 Wilson score interval with continuity correction (Newcombe, 1998).

581

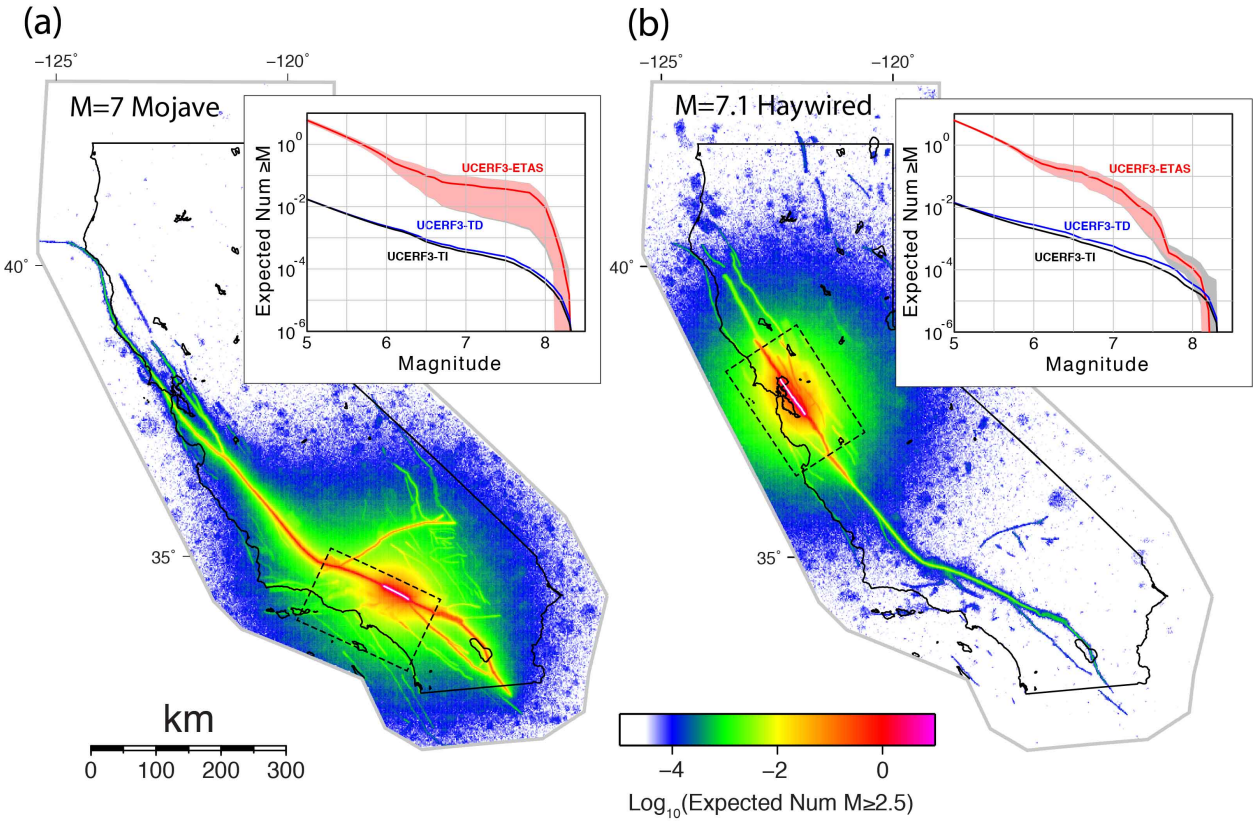

Figure 4 (a) Aftershock nucleation rates following a $M7$ earthquake on the Mojave section of the San Andreas Fault based on 2×10^5 UCERF3-ETAS simulations. Map shows the average number of $M \geq 2.5$ earthquakes nucleating in $0.02^o\times0.02^o$ cells over a 7-day period immediately following the mainshock (white line). **Inset graph**: MFD for ruptures with some part inside the dashed box defining the greater Los Angeles area. Red line is the average 7-day aftershock MFD, where the red shading represents the modeling uncertainty and the gray shading represents sampling uncertainty. Corresponding 7-day MFDs for UCERF3-TI and UCERF3-TD are black and blue lines, respectively. **(b)** Same as (a), but for a $M7.1$ mainshock on the Hayward Fault; inset graph pertains to the dashed box defining the San Francisco Bay Area.

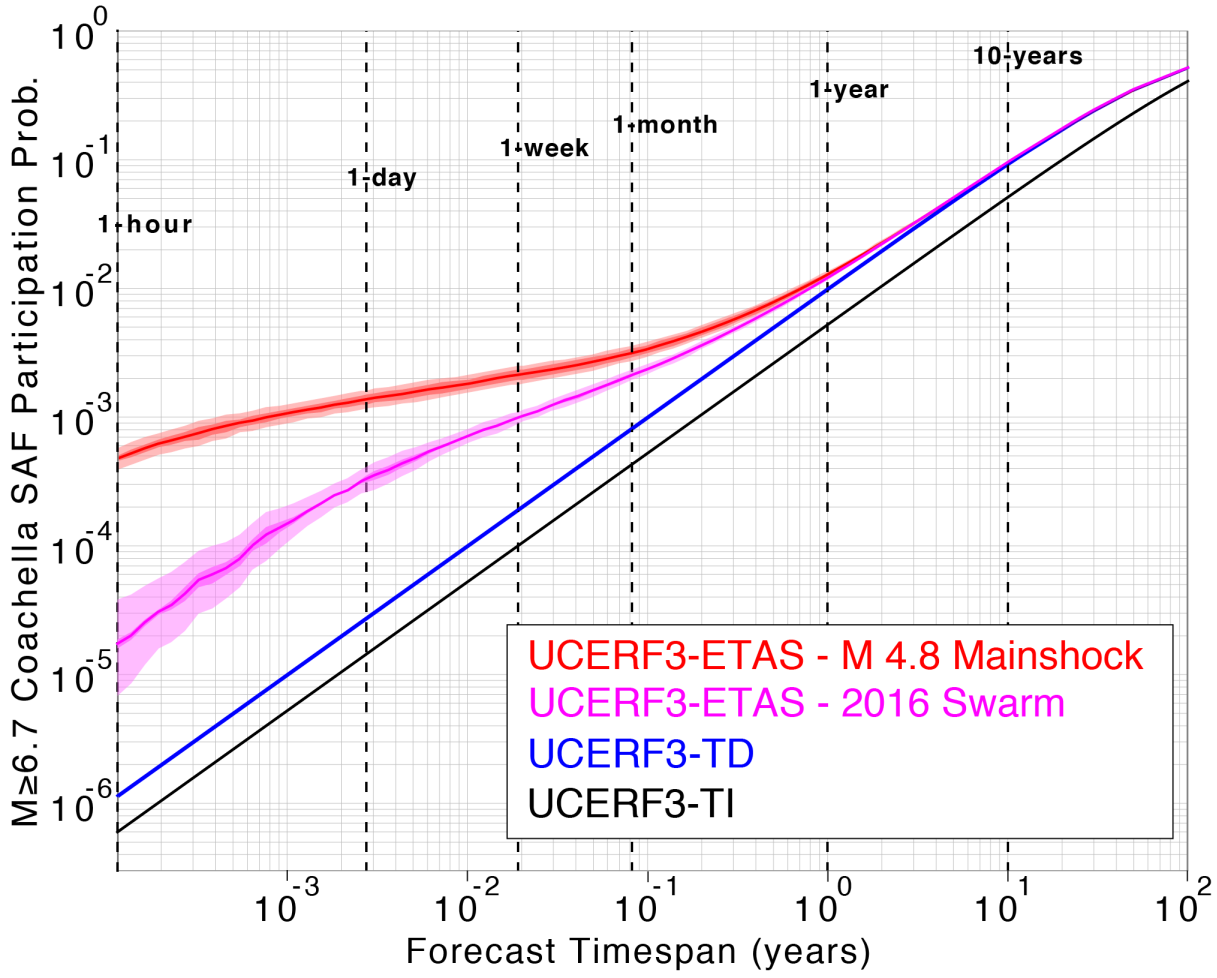

Figure 5. Probability of one or more $M \geq 6.7$ earthquakes on the Coachella section of the San Andreas Fault versus forecast timespan for UCERF3-TI (black line) and UCERF3-TD (blue line). UCERF3-ETAS probabilities following the M4.8 Bombay Beach event of Figure 2 are shown in red, and those following a 2016 swarm are shown in magenta. The latter start time at 08:30 (local time) on 9/27/2016.